Chapter

Facile NMR Relaxation Sensor for Monitoring of Biomass Degradation Products during Conversion to Biogas

Wiesman Zeev and Linder Charles

Abstract

The chemical and morphological composition of animal biowaste is known to limit the efficiency of methane production by bacterial anaerobic digestion (AD). To better understand these material limitations, we studied degradative changes in cattle manure's organic complex components chemical and morphological composition during its AD to methane. This was achieved using low field ^{1}H NMR relaxation times domain (TD) spectral mapping combined with T_1 (spin-lattice) and T_2 (spin-spin) TD of cattle manure biomass (CM) peaks assignment, starting from samples of initial freshly collected CM biomass sample followed by several time points sampling during 21 days cycle of the AD process. A T_1-T_2 relaxation TD graph giving a stable reproducible pattern of 12 peaks was generated, and assigned to different domains, whose changes during AD could be observed. These 12 peaks were assigned to TDs of crystalline nano-aggregated complexes of different degrees of crystallinity with low porosity and low hydration rate and a morphological group of amorphous domains with increased pore size, density, and higher hydration. In agreement with models of elementary cellulose fibrils, these domains were designated as three layers of cellulose consisting of interior, subsurface, and surface. The most amorphous TD volume showed good correlation with biogas production and could serve as an indicator for digestibility and cellulose conversion to a glucose intermediate during the AD process. This study demonstrated the facile and versatile usage of 2D ^{1}H NMR T_1-T_2 sensorial technology in studying complex biowaste systems, with the potential for improving CM biomass conversion efficiency into bio-methane.

Keywords: anaerobic digestion (AD), biogas, lignocellulose, ^{1}H LF-NMR relaxation, time domain (TD), cellulose crystallinity, biofilm

1. Introduction

To meet the needs of a growing world population, fossil fuels limited supply and global warming by greenhouse gas emissions, economically competitive biofuels with neutral greenhouse effects are being developed such as bacterial anaerobic digestion (AD) of biomass into methane [1, 2]. Although extensive studies have been carried out to maximize AD methane production, the major limitation is still

the relatively low yield and biomass conversion rate [3]. During AD, the bacterial enzymes hydrolyze large organic molecules into derivatives, which are then metabolized into mainly methane (55–70%) and carbon dioxide (45–30%) [1, 3]. Bacterial growth forms biofilms of colonies enclosed by extracellular polymeric substances (EPS), which films are believed to have a positive effect on bacterial activity and methane production in AD systems. However, its exact mechanism is not well known [4–7].

Cattle manure (CM) biowaste is one of the most common available feedstock for AD, but its low yield and conversion efficiency into bio-methane significantly reduces its cost effectiveness as a renewable fuel source [2, 4]. In CM, there are relatively high concentrations of cellulosic material compared to the plant forage, due to removal during forage digestion of free sugars and fats. CM contains about 40% cellulose and hemicellulose with smaller amounts of lignin, proteins, and lipids [8]. This cellulosic material is relatively resistant to bacterial AD hydrolysis [9]. This unique structural arrangement of plant cell wall cellulose and its morphological changes during AD greatly affects the hydrolysis and degradation of CM to produce biogas. Plant cell wall cellulose, contains highly ordered cellulose microfibrils bound by both inter and intramolecular forces. These cellulose microfibrils assemble into fibers with highly ordered crystalline domains, known as Iα and Iβ, interspersed within amorphous matrix regions of hemicellulose (polysaccharide) and lignin (polyphenol)—together called lignocellulose [10, 11].

Surprisingly, while there are extensive parametric studies of hydrolysis (AD and fermentation) of cellulosic biomass such as cotton and sugar cane to produce fuel such as methanol and methane [11], there is only limited research on AD of cellulosic CM. Mechanism and structural studies of fuel generation by conversion of cellulosic biomass with high cellulosic content such as cotton and sugar cane have used well-known analytical methods such as Fourier-transform infrared spectroscopy (FTIR), thermogravimetric analysis (TGA), X-ray diffraction (XRD), scanning electrons microscope (SEM), and high-resolution ^{1}H and ^{13}C nuclear magnetic resonance (NMR) [12]. These conventional methods are limited in on-line monitoring of molecular structure identification during pretreatment (e.g., acid or base hydrolysis, [13, 14], of the starting materials) and during AD. These analytical methods can either measure the crystallinity index or chemical group identification to correlate material characteristics to fuel production efficiency, i.e., methanol and methane. However, enzyme accessibility to given sites is affected not only by crystallinity and ratio of cellulose to lignin but also by specific morphological domain size, its surface structure, porosity, and their changes during hydrolysis [15, 16].

Proton low-field energy relaxation NMR (^{1}H LF-NMR) is a nondestructive method for detecting molecular and morphological changes of aggregates and complexes by two different proton relaxation times T_1 and T_2. T_1 is a longitudinal relaxation time affected mainly by the interaction between spins and surrounding environment (spin–lattice); T_2 is a transverse relaxation time affected by reactions between neighboring spins (spin–spin). T_1 and T_2 measure energy exchange within the molecular environment related to interaction energies. These values can be utilized to identify different morphological aggregate assemblies [17, 18]. Water protons (^{1}H) are readily measured by ^{1}H LF-NMR and in different environments have different energy relaxation times that can be used to identify different morphologies [19]. Within free water and liquid bulk T_1 equals T_2, therefore, measurement of differences between T_1 and T_2 can characterize liquid-solids interactions. Since T_2 relaxation time is more strongly affected than T_1, these

differences are used to measure the water-surface interactions [20–24]. Three water phases are conventionally described in solids: bound water, gel water, and capillary water. Bound water are non-freezing water chemically attached to the surface and exhibit extremely low T_2. Water in the gel pores is more mobile, but the relaxation is heavily dominated by surface interactions, giving a low T_2. The T_2 of ^1H of water in larger capillary pores is longer, but still limited and significantly lower than the bulk liquid relaxation times. The T_1 relaxation time is governed mainly by proton-surface interactions, but it is also affected by the water phase, which may be correlated to different morphologies and crystalline/amorphous ratios [23, 25].

The ratio T_1/T_2 has proven to be a valuable tool for measuring proton-molecular substrate interactions without being sensitive to material parameters such as pore density, surface area, and paramagnetic particles, which would complicate the analysis [20, 21]. T_1/T_2 can be used to quantify how morphologies affect the interaction strength and their changes under different conditions [20]. For example, this ratio was identified as a parameter of molecular substrate interactions intensity, and a measure of the activation energy of adsorption of solvents on different substrates and porous structures [21].

In this paper, we address the currently low AD conversion of cellulosic components of CM biowaste to biogas by mapping and quantification of the CM lignocellulosic nano-aggregated internal structures, at different times of AD using a novel 2D ^1H LF-NMR T_1-T_2 proton energy relaxation time-domain analysis recently developed in our laboratory. This approach to material analysis was first described in Wiesman et al. [19] for CM, wherein ^1H LF-NMR energy relaxation times T_1 and T_2 and T_1/T_2 ratios are used to form 2D and 3D chemical and morphological graphs and a corresponding T_1-T_2 TD peak assignment to material composition. In the present study, 2D ^1H LF-NMR T_1-T_2 energy relaxation mapping and T_1/T_2 ratios of absorbed water ^1H are used to identify nano-chemical and morphological structures in the CM biomass starting from cattle forage (CF) as a non-digested control, through to digested CM products and subsequent AD samples of CM under industrial mesophilic AD pilot conditions.

2. Experimental

2.1 Anaerobic digestion system

Cattle manure was collected from a district plant treating 600 tons of CM per day, from the underground preliminary tank, where the raw cattle manure is mixed with water to total solids of ~10%. AD experiments were performed in a small scale pilot plant in a laboratory at I.T.B. Ltd. Israel. The pilot plant consists of 30 L digester with temperature control, mixers, and biogas flow meters. All digestion tests were performed at batch and mesophilic conditions for a period of 21 days. Samples were taken for chemical and physical analysis before AD (time 0) and after 3, 6, and 24 h and 8 and 21 days of AD. Solids analysis of total solids (TS) and volatile solids (VS) were carried out according to standards methods [1–3]. Biogas flow was measured with Aalborg Mass Flow Meter GFM17. The flow-meter values were collected and saved by the software Real Time Viewer 1.43 Brain Child Electronics Co., Ltd.

Forage samples were collected from a feedlot of a dairy cowshed. The forage is composed of about 60% hay, 30% silage (fermented grasses and grains), and 10% grains.

2.2 ^{1}H low field NMR (^{1}H LF-NMR)

2.2.1 Sample preparation

All samples were completely dried to constant weight at 65°C. Then ground to 0.1–1 mm particle size and kept in a closed glass jars. Dried and grinded bio-waste samples were wetted to 20% moisture content (mg-water/mg-total) and placed in an NMR glass tube for conditioning at 40°C on a heating plate for 90 min prior to the ^{1}H LF-NMR test.

2.2.2 Signal acquisition

^{1}H LF-NMR measurements were carried out on a Maran bench-top pulsed NMR analyzer (Resonance Instruments, Witney, UK) equipped with a permanent magnet and a 18-mm probe head operating at 23.4 MHz. One dimensional (1D) T_1 relaxometry experiments were performed by repeating an inversion recovery step [180°– t_1] for a determined number of runs, where T_1 is varied logarithmically between runs. The t_1 is a NMR signal acquisition time [26]. The T_1 period is dominated by spin–lattice longitudinal relaxation, including possible longitudinal cross-relaxation processes. T_2 relaxometry experiments were performed using a Carr-Purcell-Meiboom-Gill sequence (CPMG) pulse sequence. This multiple sequence consists of applying a single 90° pulse followed by multiple consecutive 180° pulses. This allows measuring transverse relaxation, which results from spin–spin interactions.

The 2D cross-correlation experiments were performed by a T_1-T_2 sequence signal analysis, where the inversion recovery step [180°– t_1] is inserted prior to the CPMG sequence [20]. As in the 1D analysis for 2D, the energy relaxation processes are a T_1 period dominated by matrix longitudinal relaxation mechanisms with a possible cross-relaxation processes; while the T_2 by spin–spin transverse relaxation mechanism [17].

2.3 Computing method for analysis of 2D T_2-T_1 energy relaxation TD

The computing methodology of a reconstruction algorithm for qualitative (peak location) analysis of 2D and 3D T_1-T_2 energy relaxation graphs used in the present study is fully described in previous publications [19, 27, 28].

For quantitative analysis of the 3D T_1-T_2 vs. peak volume, we used semi-automatic software procedures for separating each peak in the graph, as described in detail in previous report [19].

2.4 Peak assignment

Peak assignment was carried out by two following approaches: spiking with standards of lignocellulose components and chemical removal of separate lignocellulosic components. Spiking of peaks was made by addition of the following standards purchased from Sigma Aldrich: cellulose fibers medium, xylan (A hemicellulosic cell wall polysaccharide, lignin, pectin.) Additional materials used in this study included: pure standards of fatty acids (acetic, propionic, butyric, and valeric acid) and internal laboratory made nano-aggregated epoxy-polymer complexes prepared from oxidized polyunsaturated fatty acid, that was previously characterized [29] and shown to consist of cross-linked aldehyde and epoxy groups, was also used as a standard. The standards were added to the dried ground samples prior to re-watering, and then water was added to the mixture to the desired moisture

content. The addition of chemical standards to CM was reflected in spiking of specific peaks/areas in the ^{1}H LF-NMR graphs, which enabled characterization of the lignocellulosic T_2-T_1 graphic peak sites in the CM [19].

Peak identification by modification of signal peaks of ^{1}H LF-NMR was made by chemically extracting/removal of lignocellulosic components according the standard approved protocols as follow: Diluted acid (HCl 2%) treatment was used for hemicellulose hydrolysis; lignin chemical degradation was based on H_2SO_4 72% according to Kalson method (ASTM D-1106) and Kurschner methodology with HNO_3 70% was used for Cellulose determination [30].

2.5 Peak volume quantification of ^{1}H

Quantification analysis of peak volume was made by testing the samples in ^{1}H LF-NMR with a fixed receiver gain (RG). RG controls the amplifying of signals acquired by the NMR. Therefore, the RG must be kept constant in order to quantify NMR signals with the same amount of amplification. All tests of cattle manure used in quantification of NMR signals were performed at RG = 3. A calibration curve of cellulose was performed by testing samples with different amount of a cellulose standard (Sigma-Aldrich C6288) with constant RG = 3.

2.6 Scanning electrons microscope (SEM)

The samples were spread onto conductive carbon tapes fixed on aluminum stubs and were sputtered with gold using Polaron Equipment Limited SEM Coating Unit E5100. The SEM micrographs were acquired in a Quanta 200 FEI Company SEM, with backscattered electron SEM imaging, secondary electron SEM imaging and energy dispersive X-ray spectroscopy (EDS) analysis.

2.7 Statistical analysis

The accuracy of 2D T_1-T_2 analysis was carried out in three repeated measurements for each of the six times (T-0, 3, 6, 24, 192, and 504 h) and analyzed with respect to the distribution of T_1 values, T_2 values, and the relative volume of each of the selected 10 peaks, i.e., peaks 1, 2, 3, 4, 5, 6, 7, 9, 10, and 11 (peak 8 was not detected in some tests and therefore omitted). We have analyzed the data of the six different times, getting a total of 18 observations for each parameter (T_1, T_2, relative volume) and a standard deviation of a statistical estimator was used to evaluate the distribution of each parameter, as described in detail in a previous paper [19].

3. Results and discussion

3.1 Characterization of CM conversion into biomethane in a mesophilic anaerobic reactor

To demonstrate the advantages of T_1-T_2 graphs generated by ^{1}H LF-NMR, for understanding AD mechanisms, we initially characterized the CM anaerobic digestion system using conventional material weight of volatile and nonvolatile solids. We measured total and volatile solids (TS and VS, respectively) in CM during 21 days of AD process (**Table 1**).

The initial amount of TS and VS loaded into the reactor was about 123 and 94 g/l, respectively. At the end of the AD process after 21 days, the amount of TS and VS was reduced by about 21 and 24% (wet weight), respectively.

Time	TS (g/l)	VS (g/l)
0 h	122.8	93.8
24 h	120.1	93.3
192 h	112.4	86.1
504 h	97.2	71.1
% Removal	20.8	24.2

Table 1.
Total and volatile solids during anaerobic digestion of cattle manure.

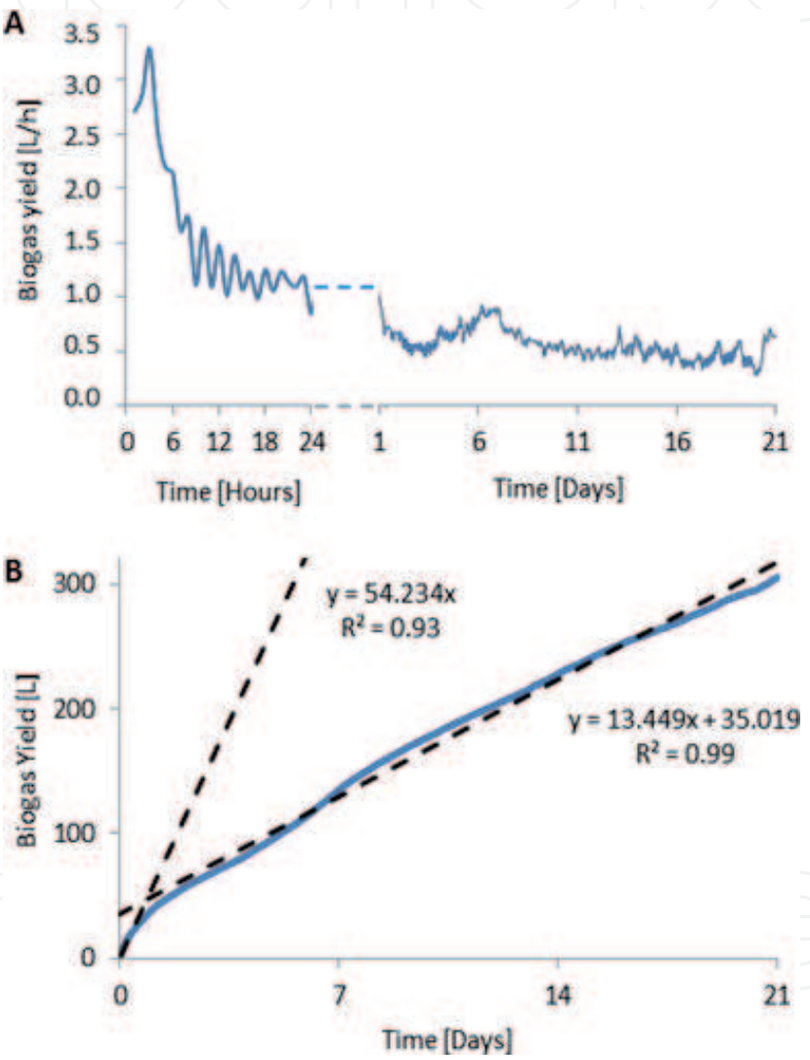

Figure 1.
Biogas yield during 21 days (504 h) of mesophilic batch AD of CM. (A) Daily biogas flow rate. The first 24 h of digestion are the most productive, in which the biogas flow rate reaches the maximum (CM-3 h) and then sharply decreases. (B) Cumulative biogas yield during 21 days of anaerobic digestion. The trend line slope of the first 24 h is much steeper than the slope of the later hours indicating the efficiency of the first 24 h.

Figure 1A shows hourly biogas flow with a typical peak seen in the first 3 h, which continually decays for 24 h. Additionally, biological enzymatic processes are often characterized with fluctuations, which are reflected in the biogas flow. **Figure 1B** shows cumulative biogas flow with a steep slope in the first 24 h and moderate slope for the later days. These biogas characteristic curves are in agreement with other studies [31]. Although the curve slope of cumulative biogas yield decreases and usually reaches a plateau after several weeks industrial AD continues

beyond the optimal biogas production time, to reduce residual product waste pathogen, odors, and pollutants to environmental none restrictive levels [2, 32].

Overall, 21 days biogas yield was 306 or 155 L per kg-VS. The biogas composition was mainly methane (57.7%) and carbon dioxide (37.7%) with a small amount of H_2S (5000 ppm), in good agreement with the prior studies [31, 33]. Biogas efficiency is commonly measured by removal of VS, which represent the organic fraction of biomass; nevertheless biomass with the same initial VS may show different amounts of VS removed [31, 33].

It should be noted that the remaining ~80% of the non-converted CM biomass contains organics that are not accessible to degrading enzymes, because of morphological or chemical barriers, and therefore are more resistant to bacterial digestion and are disposed as soil amendment.

3.2 Qualitative monitoring of CM biomass degradation in mesophilic anaerobic reactor

In the present study using 2D T_1-T_2 energy relaxation chemical-morphological mapping technology, the goal was to better understand the parameter/variable factors resulting in the relatively low conversion rate of CM lignocellulose into methane, as shown above (**Figure 1A** and **B**), and to demonstrate a potentially cost effective accurate biosensor to monitor and control the AD process. The objective is to optimize the energy conversion potential of CM by increasing bio-methane yield, by reducing chemical and morphological barriers to the degrading enzymes by using the mapping, assignment and quantification of the different CM lignocellulose nano-aggregated structures and complexes initially and at different AD time periods.

3.2.1 T_1-T_2 mapping of CM biomass decomposition during 21 days of a mesophilic anaerobic reaction

As described in the introduction by adding water, it is possible to study the porosity of polymeric materials using ^{1}H LF-NMR to generate proton T_1 and T_2 energy relaxation time domains [19, 23, 34]. T_2 spin–spin energy relaxation of water's ^{1}H provides a good indication of pores-size distribution in lignocellulosic materials [35, 36]. T_1 spin–lattice energy relaxation constant characterizes the spin-matrix interactions of ^{1}H within the lignocellulose fraction. These interactions are rationalized by hydrogen bonds of water's protons and energy exchange with the OH groups of the cellulosic components [19, 36]. To generate reproducible T_2 and T_1 energy relaxation time domain using ^{1}H LF-NMR, the water concentration in the lignocellulosic material should be an optimum needed for uniform thin-surface coatings to increase the water's ^{1}H T_1 signal, corresponding to the interaction with the outer lignocellulose complexes matrix, while simultaneously not filling pore volume, for generating well resolved signals of the spin–spin (T_2) energy relaxation of surface adsorbed water molecules. Previous studies showed that adding water to lignocellulose samples up to 20% is optimal for T_1-T_2 energy relaxation characterization [12, 19, 35].

Due to too low resolution, however, between some signals in one dimensional (1D) ^{1}H LF-NMR, energy relaxation spectra of T_2 and T_1 of lignocellulose samples, had poor peak resolution [34]. Using sparse representation methods based on PDCO (primal-dual interior method for convex objectives), we recently reported of developing a computing approach for maximization of the efficiency of inverse Laplace transformation of ^{1}H LF-NMR energy TD relaxation data to spectral graphs [19, 27]. In the present work with some modifications and adaptation, we could

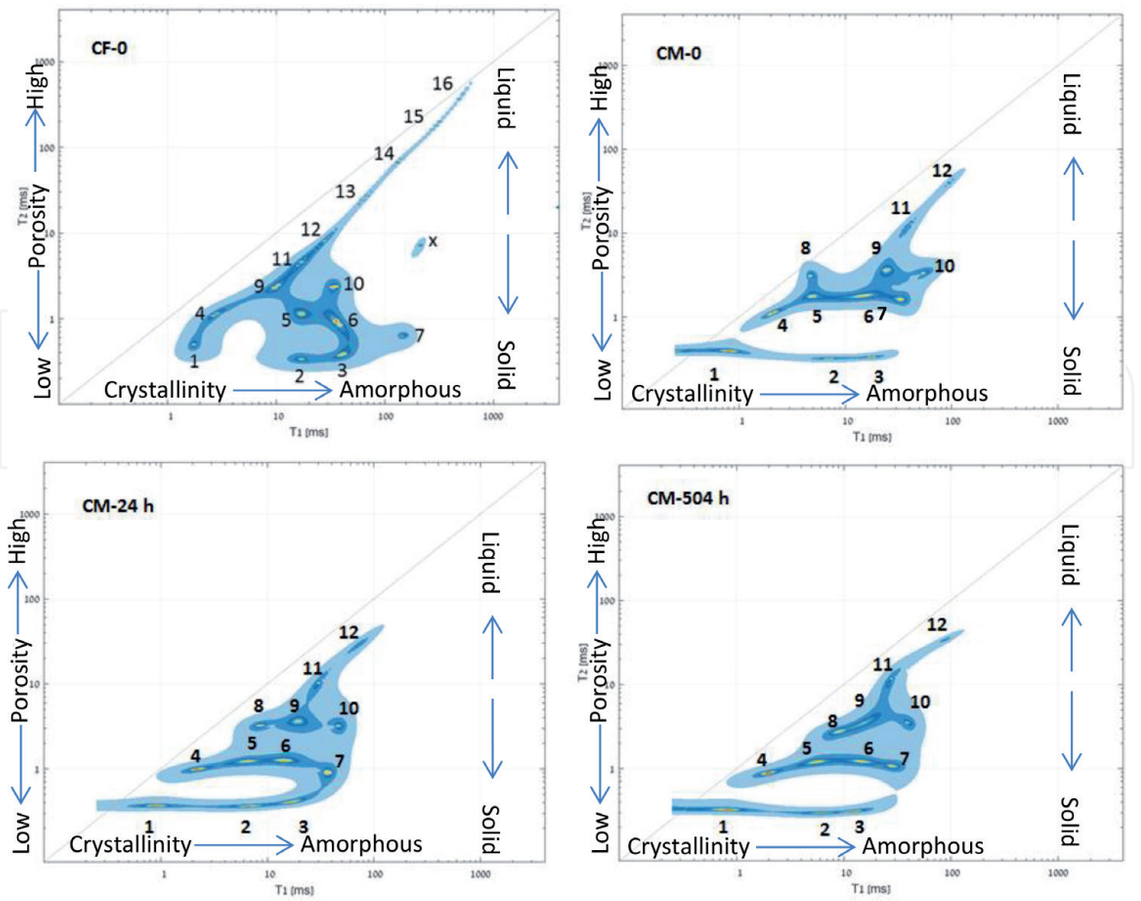

Figure 2.
Two dimensional (2D) chemical and morphology domain spectrum maps of T_1-T_2 energy relaxation signal times for graphic mapping of cattle forage (CF) and cattle manure (CM) for 21 days of AD reaction (CM-0 h; CM-24 h; and CM-504 h). T_1 correlates with the crystallinity/amorphous level of the tested complex components and T_2 correlates with the level of porosity of the complex components. Time-domain peaks 1–10 are solid and time domain peaks and above peak 11 are in liquid phase. Color ladder: Light blue – Low ^{1}H intensity; strong blue – Medium ^{1}H intensity; and yellow – High ^{1}H intensity.

specifically generate by signal reconstruction 2D graphs of T_1-T_2, with significantly improved peak resolution of lignocellulose samples described in detail in a previous study [19]. This allowed us to generate a detailed qualitative analysis of 20% hydrated complex cattle forage (CF) and CM biomass's (**Figure 2**) in morphological and chemical aggregate energy relaxation time domains (TD) and to follow their TD peaks changes during AD conversion of CM to biogas. In agreement with previous reports [13, 14] and our recent work [19], peak identification in the 2D graphs described in subsequent paragraphs, showed that the alkyl chain's ^{1}H and absorbed water's ^{1}H T_1 spin–lattice energy relaxation time changes are influenced by the different chemical structures and crystallinity levels of the cellulosic structure, and T_2 spin–spin changes are in part influenced by the porosity of the solid polymeric layer of lignocellulose. In effect, these two ^{1}H energy relaxation time values (T_1 and T_2) are providing information related to both chemical composition and morphological structure.

The 2D chemical-morphological graphics presented in **Figure 2**, described in detail below covers the following material samples:

A. Sample CF: We initiated the 2D T_1-T_2 graph study with cattle forage (CF) samples that are characterized with minimal AD, and used as a comparative control for the CM samples at different times of AD (**Figure 2** CM 0 h, CM 24 h to CM 504 h). The CF sample contains digestible and at the same basic

non-digestible chemical complexed composition as the initial CM of cellulose, hemicellulose, lignin, pectin and fatty compounds, and other components. However, with time during AD, the CM's 2D chemical and morphological spectrum shows different morphological aggregated structures of the biomass material as will be described.

B. Sample CM time zero: The second comparative sample used is fresh CM (**Figure 2**, CM-0 h). This biomass sample is demonstrating the internal cattle AD process on CF that took place in the cattle's digestive tract.

C. Sample CM time 24 h: The third sample (**Figure 2**, CM-24 h) is after 24 h of AD reaction. This sample represents the CM biomass at the end of the peak of intensive biogas production as shown in **Figure 1B**.

D. Sample CM time 504 h: The fourth and last sample (**Figure 2**, CM-504 h) is CM after 21 days of AD process, demonstrating the chemical and morphological structure at the end of the biogas production process.

3.2.2 Peaks assignment

In **Figure 2** of the samples investigated, required an intensive characterization of the CM's lignocellulose component: In effect, we assigned cellulose, hemicellulose, pectin lignin, lipid and other components and their association/localization within this T_1-T_2 map as described below. The individual ^{1}H energy relaxation time peaks for CM and cattle forage in **Figure 2** have been assigned to different water-pool interactions as a function of material chemical composition and morphological structural domains of the waters sites of absorption sites: For T_1-T_2 peak assignments, we used three approaches as described in the experimental section. The first was based on characterizing individual component standards (lignocelluloses components found in CM, including cellulose; hemicelluloses; pectin and lignin) for their peaks in a 2D T_1-T_2 graphic map. The second was based on spiking the CM or CF sample with the same aforementioned individual known standards. The third approach was based on standard chemical hydrolysis methodologies of cellulose, hemicelluloses, lignin, and pectin.

Peak assignment is also based on previous studies [19, 37–39] of similar CM biomass samples used in the present study. Cellulose is a linear biopolymer consisting of repetitive glucose units, linked by β-1,4 glycocidic bonds. Parallel cellulose chains are then assembled by hydrogen bonds and van der Waals forces into microfibrils, which are often embedded in a matrix of other polymers, such as hemicellulose and lignin. Hemicellulose is a relatively amorphous heterogeneous polysaccharide composed of a series of randomly branched polysaccharides [4, 8, 40], of which the short branch chains usually contain different monomers such as xylose, mannose, galactose, rhamnose, and arabinose. In addition, hemicellulose interacts with cellulose, pectin, and lignin giving a network structure resistant to hydrolysis [4, 28]. Lignin is a large, complex aromatic heteropolymer present in cell walls made of different phenyl propane alcohols. The content and composition of lignin varies between plant species, and functions to increase the strength of plant cell wells. Pectin known as a gelling agent is a structural heteropolysaccharidein the primary cell walls and is particularly abundant in the non-woody parts of terrestrial plants, and its content is relatively high in forage [36].

In our study CF and CM described below, the lignocellulosic biomass is divided into three morphological domains D1 (peak groups 1, 2, 3), D2 (peak groups 4, 5, 6, 7), and D3 (peak groups 9, 10, peak 8) is missing in CF sample and will be discussed later on.

Each domain has similar T_2 relaxation times and is divided to sub-domains, of individual peaks, by the different T_1 values. Other non-lignocellulosic components, such as free sugars and fatty acid compounds, are assigned domains D4 (peak group 11) and D5 (peak groups 12–16), respectively.

Based on the T_1-T_2 mapping strategy for lignocellulose complex materials described above, to characterize internal morphology and chemical structures, it is possible to explain the differences between each T_1-T_2 peaks, and to suggest a rational assignment for the first ten lignocellulosic associated peaks found in the different CF and CM samples studied. A brief peak assignment is listed below:

Peak 1 in **Figure 2** has the fastest, in effect shortest, T_2 and T_1 energy relaxation times. This is rationalized by the smallest matrix pore size (lowest T_2) and thus the strongest water ^{1}H interaction with the internal surface of the nano-aggregate most crystalized cellulosic domain (lowest T_1). Considering the 2D graphic mapping of cellulose standard [26] and the cellulose specific chemical hydrolysis test, we assigned peak 1 to the cellulose's mostly crystalline interior domain of the lignocellulose fiber complex. This is in good agreement with the state of art for lignocellulose models [4, 28]. For peak 10 with the longest T_2 and T_1 is well associated with the localization to the amorphous cellulose standard as well as spiking tests using this standard [19], which suggests an assignment to the most amorphous cellulose outer surface domain of the lignocellulose fibers that correlates with the elementary cellulose microfibril model [28]. Interestingly, since the forage sample is rich in young vegetable grasses dominated by primary cell wall, and high in pectin [4], it is highly hydrated as it contains relatively higher amounts of amorphous cellulose domains as seen by the peak heights in forage (**Figure 2**, CF) compared to the CM (**Figure 2**, CM).

Peaks 2 and 3 having a longer T_1 than peak 1 can be rationalized as a reduction of water proton interaction strength with part of the interior crystalline cellulose domain's surface consisting of cellulose partially associated with hemicelluloses and pectin chains.

Peak 4 is assigned as a subsurface second layer [28]. It consists of para-crystalline morphology.

Peak 5 fits well to the standard and spiking localization tests of oxidized polyunsaturated fatty acid domain [26]. This standard is rich in aldehyde end groups and will be discussed later.

Peak 6 is assigned to medium-hydrate para-crystalline nano-aggregated cellulose complex [28]. A relatively higher degree of hydration typical for this peak is explained because of the relatively open hemicellulose "loop chains" that may absorb more water [28, 34] in comparison to peak 4.

Peak 7 is assigned to a hydrated partially amorphous cellulose subsurface layer.

Peaks 8, 9: Based on the polyunsaturated fatty oxidized standard localization analysis and data from relevant literature reports [3], peak 8 is assigned to a well-developed outer surface microbial epoxy hydrophobic nano-aggregated domain. These peaks as well as peak 5 are generated not by water ^{1}H but mainly from aliphatic chains characterized by T_1 equal to T_2. Considering lignocellulose components standard spiking, peak 9 domain is assigned to a semi-hydrated surface amorphous nano-aggregated fraction of depolymerized cellulosic oligosaccharide products, associated with hemicellulose and trapped lignin.

Peak 10: Due to its relatively long T_1 and T_2 energy relaxation times and localization of most amorphous cellulose standards, we assigned peak 10 to a high amorphous packing, and in agreement with the literature [4, 32] to an amorphous cellulosic moiety with an outer hydrated surface on a highly amorphous domain of cellulose of the CM components with the potential for hydrolysis and release of free sugars (glucose), shown in peak 11, as identified by standards and spiking tests [19].

Peak 11: Based on standard and spiking tests, peak 11 is assigned to monosaccharide free sugar subdomains.

Peak 12 is attributed to disaccharide free sugars.

Peaks groups 13–15 appear only in the spectrum map of CF. They are assigned by standards test, to fatty acids with different carbon chain lengths and the alkyl chain's degree of unsaturation. These fatty acids were easily absorbed in the cattle intestine system and/or metabolized by the internal anaerobic bacteria digestion activity.

Based on the above peak assignments: CF sample in **Figure 2** shows the T_1-T_2 relaxation time graphic map of the cattle forage biomass, and is compared to the CM biomass, as a relatively non-anaerobic digested organic control biomass material for visualization of chemical and morphological spectrum changes due to cattle rumen bacterial digestive activity and absorption of cattle feeding material components. It can be seen in **Figure 2** that CF sample is much richer in the free sugars (peak 11) in comparison to CM-0 h. Furthermore, triacylglycerol and all graphic spectrum peaks of conventional vegetable oils and fatty acids (peaks 14–16 shown in **Figure 2**) is obtained only in the CF sample and is totally missing in the graphic spectrum of CM samples. The assignment of all these T_1-T_2 peaks was confirmed by graphic mapping of sugars and fatty acids standards previously reported by us [19] for CM biomass. At the lower part of the diagonal, in **Figure 2** at first view CF, graphic map may show a different pattern of peak distribution that can be rationalized by the metabolism process of CM sample. However, following a deeper view, it can be observed that CF has many basic similarities to CM-0 h. A relatively small pore-size material domain (in effect a low T_2) within the suggested interior of lignocellulose crystalline layer (peaks 1, 2, and 3) can be seen in the **Figure 2** graphic map of CM and CF as well. Other domains represent a second intermediate porosity layer representing the subsurface (peaks 4, 5, 6, and 7) of the elementary cellulose microfibril model [28], followed by a more increased pore-size layer of the fibril surface assigned to peaks 9 and 10.

Interestingly, in CF, T_1-T_2 energy relaxation time graphic map (**Figure 2**, CF) peaks 5, 6, and 7 are partly shifted to increased T_1 (due to higher absorption of water and longer ^{1}H energy relaxation times) in comparison to CM energy relaxation graphic map (**Figure 2**, CM-0 h). This signal shift to relatively longer T_1 energy relaxation times suggests changes of the molecular environment of the cattle forage nano-aggregated complex may be explained by the significantly higher content of pectin in forage sample [37, 38] known to have a stronger water interactions with gel-like properties (as discussed previously). All these significant spectral T_1-T_2 peak shifts/changes between CF vs. CM samples, indicating that the present 2D relaxation mapping system is able to distinguish between different molecular morphologies and supramolecular interactions. This is in agreement with standards localization and spiking analysis described above for CM, with variations rationally suggested to be assigned to high pectin concentration environments associated with cellulose, since the forage sample is rich in young vegetable grasses dominated by primary cell wall, high in pectin [36] that is highly hydrated and contains relatively high amorphous cellulose domains. Furthermore, peak 8 is missing in forage biomass sample (**Figure 2**, CF) in comparison to CM relaxation map (**Figure 2**, CM-0 h, CM-24 h, and CM-504 h), which is generate by ^{1}H on alkyl chains present only in CM due to developed anaerobic bacterial biofilm during digestion. Thus some T_1-T_2 peaks identify domains related to materials processed and formed by digestion in the cattle's rumen by anaerobic microbial activity. In effect for CM, the forage biomass underwent an AD process in the cattle rumen.

In the AD process of CM, a significant degradation is observed for cellulose fibers and a significant microbial colonization layer (biofilm) presence, which is assigned to peak 8. In the section on quantitative determination of ^{1}H proton density per peak, we can show biofilm growth beyond CM-0 h and CF samples, in CM-24 h and 504 h samples. This pattern of both surface cellulose degradation and increase of an extracellular polysaccharide (EPS) thick biofilm layer is expected [19]. The standard localization test of oxidized polymers rich in aldehydes support this material assignment to peak 8 T_1-T_2 at 4.32–2.71 ms.

3.2.3 Monitoring of T1/T2 ratio of CM biomass T_1-T_2 TD

In this study, ^{1}H T_1 and T_2 energy relaxation times of absorbed water protons are used to characterize different morphological domains in CM and how these domains change during AD. As described above, the different morphological domains within CM are compared, and the changes they undergo, by a 2D relaxation graphic map of T_1-T_2 peaks. Another important aspect we would like to characterize is the interactive strength of the water-proton absorption within the different CM morphologies. In effect with respect to the different degrees of crystallinity, the strength of the water's proton absorption on a given morphology may be correlated to the degree of crystallinity of the substrate. As described in the introduction and further below, one measure of interactive strength is the T_1/T_2 ratio of a given T_1-T_2 peak.

The ^{1}H relaxation times of absorbed water T_1 are generally larger than T_2 [21], and this is also seen in the present study of CM. In the T_2 vs. T_1 2D graphs (**Figure 2**) of undigested CM (CM-0 h), all peaks are with T_1 equal or larger than T_2, and are thus below the dotted diagonal ($T_1/T_2 = 1$) in the 2D map. As described above, $T_1 = T_2$ relaxation times in bulk water, but in absorbed water the ^{1}H relaxations are $T_1 > T_2$ and thus $T_1/T_2 > 1$. This can be seen in **Table 2** giving the T_1/T_2 ratio for different morphological sites in the 2D CM T_1-T_2 relaxation graphs at different AD times.

The values of T_1/T_2 in **Table 2** can be correlated with the strength of the interactions between ^{1}H H_2O and the surface, which can be rationalized in our study by the degree of crystallization and the number of –OH on the cellulose available for interaction with the absorbed water molecule. Thus, the higher the T_1/T_2 value the stronger the interaction for a given morphological domain due to the greater reduction of T_2 than T_1 when going from bulk water to adsorbed water on external and porous surfaces.

One set of interesting results is the comparison between peaks 1, 2 and 3, which vary from highly crystalline to semi-hydrated crystalline respectively, in the T_1-T_2 graphs (**Figure 2**) in terms of T_1/T_2 values. Each of these peaks is associated with a crystalline cellulose domain, wherein the each of these crystalline domains is enclosed in different environments. In this line, the T_2 relaxation values are relatively constants and the T_1 values increase significantly, such that the T_1/T_2 ratio

Time	Peak										
	1	**2**	**3**	**4**	**5**	**6**	**7**	**8**	**9**	**10**	**11**
0 h	2.21	20.81	54.60	2.00	3.89	9.15	23.16	1.60	7.54	19.92	3.61
24 h	2.20	17.35	37.30	2.25	4.59	12.66	37.06	2.97	4.71	13.49	2.81
504 h	2.51	23.29	38.75	2.38	4.73	9.98	25.04	3.44	4.00	11.10	2.54

Table 2.
T_1/T_2 ratio [ms/ms] of different morphological sites in 2D T_1-T_2 relaxation time of CM.

goes from in the range of 2–20–55 for peaks 1, 2, and 3, respectively. This increase is attributed to increasing T_1 values, brought about by lower interaction strength of the absorbed water ^1H with the local environment which we hypothesis is due to changes in the environment of the crystalline cellulose nano/micro morphologies, which lowers interactive strength and increases T_1. This same trend is seen at all stages of the AD for T_1-T_2 domains 1, 2, and 3. In T_1-T_2, peaks 5, 6, and 7 which are less crystalline and significantly amorphous, wherein the T_2 stays approximately constant the same trend is seen with increasing T_1 values with the T_1/T_2 ratio going from 4 to 9 to 23, respectively.

If we look at peaks 3, 6, and 9 (crystalline interior, semi-hydrated sub surface, and amorphous surfaces, respectively), which go from crystalline to less crystalline to highly amorphous morphologies, wherein the T_1 is relatively constant the T_1/T_2 ratio decreases from 55, 9, and 7.5 at time zero which at time 21 days goes from 38.7, 10 to 4, the trend in T_1/T_2 is similar and indicates that T_1/T_2 is changing because of the increasing strength of interaction with the given morphology, which appears to be the strongest with the more crystalline (peak 3) and decreasing with the increase in the more amorphous morphologies and different chemical compositions such as hemicellulose and lignin. This reduction in the strength of the interaction may correspond to the increases in T_2 in the amorphous regions.

If we look at T_1-T_2 domains 7, 10, and 11 (amorphous sub-surface, highly amorphous surface, and free sugars, respectively) with a relative similar T_1, the T_2 values increase and thus T_1/T_2 ratios decrease, which may be due to decrease in the interactive strength of adsorbed ^1H water interactions with the surrounding environment due to decreases in cellulosic chains and thus decreasing hydrogen bonding interactions.

If T_1 value and T_2 both increase by the same factor—the ratio T_1/T_2 does not change. For example, peaks 7 (amorphous sub-surface) and 3 (crystalline interior, described above in Section 3.2.2) have high and similar pattern of T_1/T_2 ratio from 24 to 504 h (in **Table 2**), indicating similar strengths of water adsorption though differences in morphology, wherein other components in the surrounding environments may affect the results by competitive interactions with the ^1H interactions.

3.3 SEM of CM biomass fibers changes during AD

To further support the conclusions on chemical-morphological arrangements in CF and CM, we did SEM analysis to visually observe changes of biomass fibers during 21 days of mesophilic anaerobic reaction (AD). In **Figure 3**, degradation of cellulose fibers (Black arrows) is readily seen at magnification ×1000 and ×5000. Developed bacterial biofilms are seen at magnification ×20,000 (**Figure 3**, black dashed arrows): In the forage, there are only isolated bacterial colonies most likely on most of the amorphous surface. In the two low magnification SEM photos (×1000 and ×5000), clear intact cellulosic fibers can be easily seen (**Figure 3**). In the relatively higher SEM magnification of ×20,000, small and non-developed and non-continuous spots/layer of bacterial biofilm could be observed. This biofilm can be explained by the silage process that the forage passed before being used as CF.

In the sample of CM-0 h, partially digested lignocellulose fibers are clearly seen and a significant bacterial biofilm layer covering the surface is seen in all three SEM magnification images.

The SEM images of CM-24 h show a similar pattern of fibers digestion and a thicker growing continuous bacterial biofilm layer that covers the entire surface. Following 504 h (21 days) of AD, the lignocellulose fibers seems to be most degraded in the two low SEM magnification (×1000 and ×5000) and the biofilm layer is also observable as in the sample of CM-24 h.

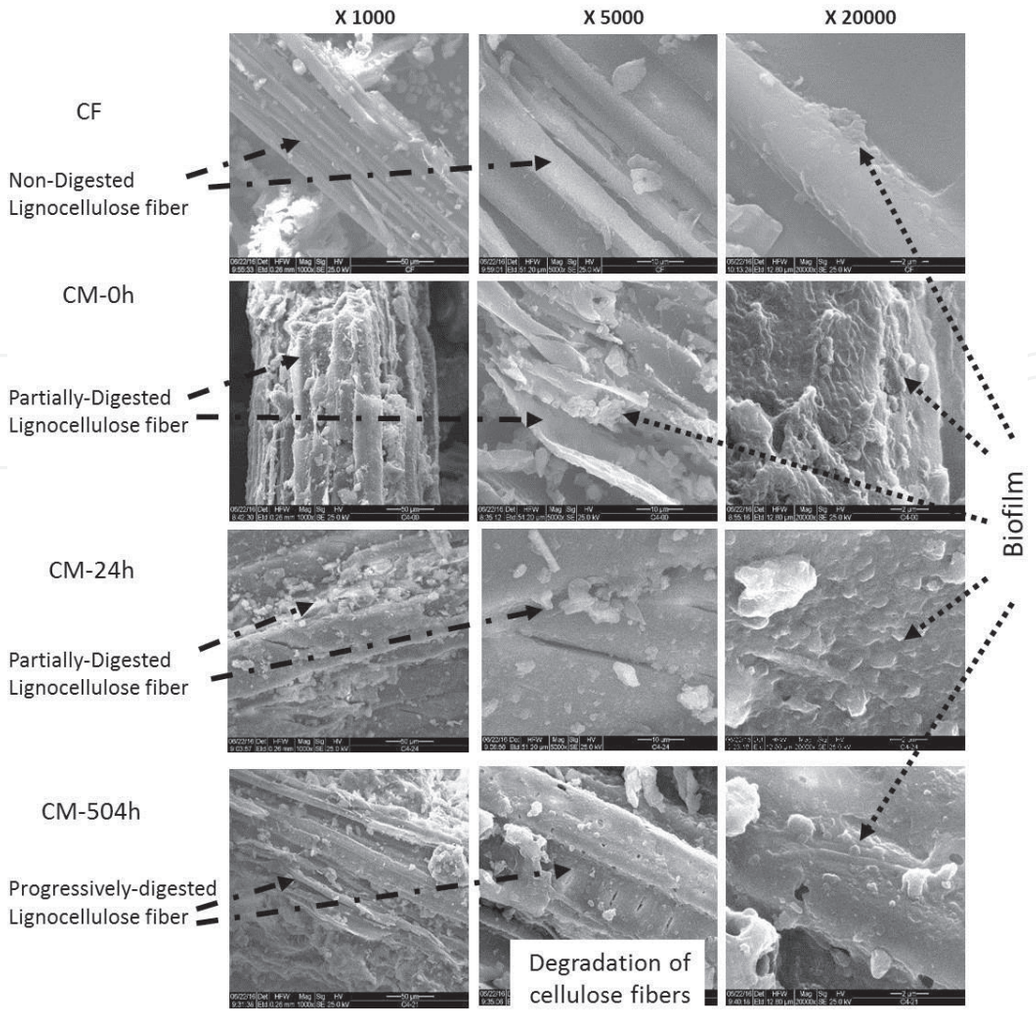

Figure 3.
Scanning electrons microscope (SEM) images of cattle forage (CF) and cattle manure (CM) at different times of anaerobic digestion (AD): 0, 24, and 504 h. different stages of lignocellulose digestion are shown by arrows in left side and anaerobic bacterial biofilm is shown by arrows in the right side of the figure.

3.4 Quantitative monitoring of accessible amorphous cellulosic components during 21 days of mesophilic anaerobic reactions

To carry out a quantitative analysis of the results based on the 2D T_1-T_2 relaxation study: We developed a computing protocol (described in details in supplemental section S2), which enabled the quantification of proton (^{1}H) concentrations within all peak domains measured during the anaerobic digestion process (**Table 3**).

The results show that proton populations of peaks 1 and 4 assigned as most crystalline cellulose nano-aggregated complexes are stable during most of the digestion process, while peak 1 increased during the last period near to 21 days (**Table 3**).

The relative volumes of the most amorphous peaks 7 and 10 are considerably reduced, which we suggest to be rationalized is due to the fact that these two amorphous morphologies are most readily subjected to bacterial degradation. The proton population of peaks 5 and 8, assigned to oxidized aggregated structures of bacterial EPS biofilm (shown in S3), show a general increase from the initial stage to the end of AD process at 21 day (**Table 3**).

Proton population of peaks 11, assigned to free sugars that are continuously released from the amorphous fractions of the nano-aggregated cellulosic complexes and then degraded to volatile fatty acids to yield the final biogas product, have a relatively stable steady ^{1}H state concentration during the anaerobic process (**Table 3**).

Time	Peak										
	1	2	3	4	5	6	7	8	9	10	11
0 h	20.58	8.17	6.69	21.54	6.16	13.13	14.12	2.07	2.71	4.38	0.62
24 h	21.58	11.57	9.46	16.66	8.65	11.57	10.82	3.23	6.47	2.16	1.06
504 h	25.94	10.15	8.31	21.76	9.74	9.13	7.05	5.73	6.63	1.32	1.26

Table 3.
A peak's relative volume (%) compared to all the peaks within a 3D T_1-T_2 relaxation map of cattle manure during anaerobic digestion.

3.5 Description of the amorphous cellulose component's peak 10 and its correlation with equivalent changes of CM with biogas production rate during 21 days of AD

As a follow up of our previous report [19] demonstrating the usefulness of peak 10 for monitoring of amorphous cellulose equivalent (ACE), we now correlated it with biomethane production rate during 21 days of mesophilic anaerobic reaction. Peak 10 has the longest T_1 and T_2 relaxation times of all others lignocellulosic domains. Indicating that this domain is composed of the most loosely packed and less ordered aggregate structure, such that water molecules have lower interaction forces with the morphological surfaces allowing higher water mobility during energy exchange with cellulose fibers surface. Furthermore, during AD, this peak 10 domain being amorphous allows better access of the water solubilized hydrolytic enzymes. Hence, the domain represented by peak 10 are more readily degradable suggesting it is readily degraded to free sugars that are further hydrolyzed to short chain volatile fatty acids such as acetate, propionate, butyrate that are used by methanogenic bacteria to generate methane.

Taking advantage of the ability to quantify T_1-T_2 relaxation signals, with respect to ^{1}H concentration, a good correlation between peak 10's volumes with the biogas flow was achieved (**Figure 4**). Within the first 24 h, when biogas flow significantly increases to a maximum level, peak 10's volume decreases to a lower level compared to the original values. Along the entire period of 21 days of the AD process, this inverse correlation of peak volume to gas flow is clearly demonstrated. This finding enables us to suggest that peak 10 as an indicator for digestibility of cellulosic components in complex chemical and morphological mixtures.

As was already demonstrated in our previous paper [19], the signal volume of amorphous cellulose at peak 10 shows a highly linear fit in our 2D T_1-T_2 system.

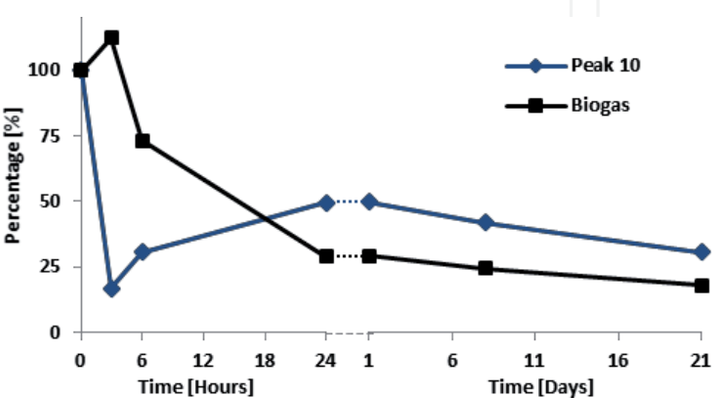

Figure 4.
Relative biogas flow rate and signal volume of peak 10 during 21 days of AD. Left side of the curve is the first 24 h of AD and the right side is from 24 to 504 h. there is an inverse match between the volume of peak 10 and the biogas flow suggesting peak 10 is the amorphous cellulose degraded straight forward to biogas.

Time	Peak 10 signal [Intensity (AU)]	ACE in a sample (mg)	Total ACE (% Dry)	Total ACE in digester (g)
CF	2655	483	16.1	—
CM 0 h	748	136	4.53	117
CM 3 h	133	24.2	0.81	20.8
CM 6 h	250	45.4	1.51	39.0
CM 24 h	410	74.5	2.48	62.6
CM 192 h	332	60.4	2.01	47.6
CM 504 h	264	48.0	1.60	32.7

Table 4.
Amorphous cellulose equivalent (ACE) of cattle manure during CM anaerobic digestion and of forage. (AU is in arbitrary units).

Thus indicating every 5.5 signal units of peak 10 in the 2D relaxation map are equivalent to 1 mg of amorphous cellulose. Therefore, we can calculate the amorphous cellulose equivalent (ACE) mg of cellulosic biomass as shown in **Table 4**.

The concentration of ACE in forage (CF) is much higher than in CM because it mostly raw none-degraded biomass. It is clearly obtained in **Table 4** in term of signal intensity (represented by volume) of peak 10 is dramatically high (X3.5) in the control CF sample than in CM 0 h sample. During the first hours of AD process of CM, peak 10 intensity significantly declines after which until the end of the process at 21 days the signal intensity mildly fluctuated. Similar pattern of fluctuation is found in absolute values (mg) and also in percentage of ACE. It should be noticed that although ACE of CM is reduced during AD, it keeps a low value due to constant degradation of the inner layer of lignocellulose that creates new amorphous regions. The total ACE of CM before digestion was 117 g and immediately decreases to its minimum value of 20.8 g due to a peak in bacterial activity and biogas production then slightly increases and fluctuates for the rest of the digestion period due to consumption-production fluctuation rates.

4. Conclusion

We demonstrated the monitoring of the chemical and morphological changes of CM biomass during anaerobic mesophilic digestion in a biogas production process, by T_1-T_2 energy relaxation time graphs generated by signal reconstruction from LF ^{1}H NMR. Graphical peak changes in 2D LF ^{1}H NMR monitored the rate of crystallinity and porosity changes of the CM lignocellulosic biomass, and provided a better understanding of its conversion to biogas mechanism. This demonstrated the versatile usage of 2D ^{1}H NMR T_1-T_2 technology in studying complex chemical and morphological systems, with the practical potential for improving biomass conversion efficiency into biomethane.

In addition to accurate qualitative mapping of the different energy relaxation time domains (TD) and subdomains of the different nano-aggregates in CM biomass complexes, a detailed peak assignment to chemical and morphological structures was formulated. The proton NMR relaxation TD sensor provided also quantitative data of the changes of the key amorphous cellulose morphology that is accessible to bacterial digestive enzymes to release free sugars that are fermented by methanogenic bacteria to produce the final product of bio-methane and carbon

dioxide. Furthermore, the facile NMR TD sensor also provides chemical and morphological information on the growth and changes of bacterial biofilm during the anaerobic digestion (AD) of the CM biomass. This information may be used to study optimal preconditioning of samples to maximize bio-methane yield and to identify optimal termination times of the AD process.

Acknowledgements

We would like to thank Dr. O. Levi and Dr. D. Benson from the Open University for the mathematical and statistical backup and support of this study. We would also like to thank Mr. Natan Ayallon, Ms. Maysa Resende, Dr. J. Abramovich, Ms. S. Kravcik, and all the members of the Phyto-Lipid Biotechnology Lab (PLBL) for the intensive technical assistance. This study was supported by a grant from the Israeli Ministry of Science Technology and Space.

Competing financial interests

The authors declare no competing financial interests.

Author details

Wiesman Zeev* and Linder Charles
Phyto-Lipid Biotechnology Laboratory (PLBL), Department of Biotechnology Engineering, Energy Engineering Unit, Faculty of Engineering Sciences, Ben Gurion University of the Negev, Beer Sheva, Israel

*Address all correspondence to: wiesman@bgu.ac.il

References

[1] Chynoweth DP, Owens JM, Legrand R. Renewable methane from anaerobic digestion of biomass. Renewable Energy. 2001;**22**:1-8

[2] Holm-Nielsen JB, Al Seadi T, Oleskowicz-Popiel P. The future of anaerobic digestion and biogas utilization. Bioresource Technology. 2009;**100**:5478-5484

[3] Yu Z, Morrison M, Schanbacher FL. Production and utilization of methane biogas as renewable fuel, chapter 20. In: Vertès AA, Blaschek HP, Yukawa H, Qureshi N, editors. Biomass to Biofuels: Strategies for Global Industries. Hoboken, NJ, USA: John Wiley & Sons; 2010. pp. 403-433

[4] Appels L, Lauwers J, Degrève J, Helsen L, Lievens B, Willems K, et al. Anaerobic digestion in global bio-energy production: Potential and research challenges. Renewable and Sustainable Energy Reviews. 2011;**15**:4295-4301

[5] Dumitrache A, Wolfaardt GM, Allen DG, Liss SN, Lynd LR. Tracking the cellulolytic activity of *Clostridium thermocellum* biofilms. Biotechnology for Biofuels. 2013;**6**:1-14

[6] Fernández N, Díaz EE, Amils R, Sanz JL. Analysis of microbial community during biofilm development in an anaerobic wastewater treatment reactor. Microbial Ecology. 2008;**56**:121-132

[7] Langer S, Schropp D, Bengelsdorf FR, Othman M, Kazda M. Dynamics of biofilm formation during anaerobic digestion of organic waste. Anaerobe. 2014;**29**:44-51

[8] Chen S, Liao W, Liu C. Value-Added Chemicals from Animal Manure. Richland, WA, USA: Pacific Northwest National Laboratory; 2003. pp. 1-135

[9] Taherzadeh MJ, Jeihanipour A. Recalcitrance of lignocellulosic biomass to anaerobic digestion, chapter 2. In: Mudhoo A, editor. Biogas Production: Pretreatment Methods in Anaerobic Digestion. New York, USA: Wiley; 2012. pp. 27-54

[10] Ding S, Himmel ME. The maize primary cell wall microfibril: A new model derived from direct visualization. Journal of Agricultural and Food Chemistry. 2006;**54**:597-606

[11] Quiroz-Castañeda RE, Folch-Mallol JL. Hydrolysis of biomass mediated by cellulases for the production of sugars, chapter 6. In: Quiroz-Castañeda RE, Folch-Mallol JL, editors. Sustainable Degradation of Lignocellulosic Biomass- Techniques, Applications and Commercialization. Rijeka: InTechOpen; 2013. pp. 119-155

[12] Bernardinelli OD, Novotny EE, de Azevêdo ER, Colnago LA. Analyses of biomass products by nuclear magnetic resonance spectroscopy, chapter 6. In: Vaz Jr. S, editor. Analytical Techniques and Methods for Biomass. Cham: Springer International Publishing; 2016. pp. 143-172

[13] Chandel AK, Antunes FA, Anjos V, Bell MJ, Rodrigues LN, Polikarpov I, et al. Multi-scale structural and chemical analysis of sugarcane bagasse in the process of sequential acid–base pretreatment and ethanol production by *Scheffersomyces shehatae* and *Saccharomyces cerevisiae*. Biotechnology for Biofuels. 2014;**7**:1-17

[14] Gómez X, Diaz MC, Cooper M, Blanco D, Morán A, Snape CE. Study of biological stabilization processes of cattle and poultry manure by thermogravimetric analysis and 13 CNMR. Chemosphere. 2007;**68**:1889-1897

[15] Park S, Baker JO, Himmel ME, Parilla P, Johnson DK. Cellulose crystallinity index: Measurement techniques and their impact on interpreting cellulase performance. Biotechnology for Biofuels. 2010;**3**:1-10

[16] Silverstein RM, Webster FX, Kiemle DJ, Bryce DL. Carbon-13 NMR spectrometry, chapter 4. In: Spectrometric Identification of Organic Compound. New York, USA: John Wiley & Sons; 2014. pp. 204-244

[17] Hills B, Benamira S, Marigheto N, Wright K. T 1-T 2 correlation analysis of complex foods. Applied Magnetic Resonance. 2004;**26**:543-560

[18] Song Y, Venkataramanan L, Hürlimann M, Flaum M, Frulla P, Straley C. T1–T2 correlation spectra obtained using a fast two-dimensional Laplace inversion. Journal of Magnetic Resonance. 2002;**154**:261-268

[19] Wiesman Z, Linder C, Resende MT, Ayalon N, Levi O, Bernardinelli OD, et al. 2D and 3D Spectrum graphics of the chemical-morphological domains of complex biomass by low field proton NMR signal analysis. Energy & Fuels. 2018;**32**:5090-5102

[20] McDonald P, Korb J, Mitchell J, Monteilhet L. Surface relaxation and chemical exchange in hydrating cement pastes: A two-dimensional NMR relaxation study. Physical Review E. 2005;**72**:011409

[21] D'Agostino C, Mitchell J, Mantle MD, Gladden LF. Interpretation of NMR relaxation as a tool for characterising the adsorption strength of liquids inside porous materials. Chemistry - A European Journal. 2014;**20**:13009-13015

[22] Berman P, Meiri N, Colnago LA, Moraes TB, Linder C, Levi O, et al. Study of liquid-phase molecular packing interactions and morphology of fatty acid methyl esters (biodiesel). Biotechnology for Biofuels. 2015;**8**:1-16

[23] Cox J, McDonald PJ, Gardiner BA. A study of water exchange in wood by means of 2D NMR relaxation correlation and exchange. Holzforschung. 2010;**64**:259-266

[24] Foston M, Ragauskas AJ. Changes in the structure of the cellulose fiber wall during dilute acid pretreatment in Populus studied by 1H and 2H NMR. Energy & Fuels. 2010;**24**:5677-5685

[25] Meng X, Foston M, Leisen J, DeMartini J, Wyman CE, Ragauskas AJ. Determination of porosity of lignocellulosic biomass before and after pretreatment by using Simons' stain and NMR techniques. Bioresource Technology. 2013;**144**:467-476

[26] Berman P, Levi O, Parmet Y, Saunders M, Wiesman Z. Laplace inversion of low-resolution NMR relaxometry data using sparse representation methods. Concepts in Magnetic Resonance Part A. 2013b;**42**:72-88

[27] Campisi-Pinto S, Levi L, Benson D, Cohen M, Resende MT, Saunders M, et al. Analysis of the regularization parameters of primal-dual interior method for convex objectives applied to 1H low field nuclear magnetic resonance data processing. Applied Magnetic Resonance. 2018;**49**:1129-1150

[28] Berman P, Leshem A, Etziony O, Levi O, Parmet Y, Saunders M, et al. Novel 1 H low field nuclear magnetic resonance applications for the field of biodiesel. Biotechnology for Biofuels. 2013a;**6**:1-20

[29] Berman P, Meiri N, Linder C, Wiesman Z. 1H low field nuclear magnetic resonance relaxometry for probing biodiesel autoxidation. Fuel. 2016;**177**:315-325

[30] Reid JD, Lynch D. Cellulose Analysis. Industrial and Engineering Chemistry, Analytical Edition. 1937;**9**:570-573

[31] Rico C, Rico JL, Tejero I, Muñoz N, Gómez B. Anaerobic digestion of the liquid fraction of dairy manure in pilot plant for biogas production: Residual methane yield of digestate. Waste Management. 2011;**31**:2167-2173

[32] Gerardi MH. The Microbiology of Anaerobic Digesters. Hoboken, NJ, USA: John Wiley & Sons; 2003. pp. 1-192

[33] Nasir IM, Mohd Ghazi TI, Omar R. Anaerobic digestion technology in livestock manure treatment for biogas production: A review. Engineering in Life Sciences. 2012;**12**:258-269

[34] Ono H, Shimaya Y, Sato K, Hongo T. 1H spin-spin relaxation time of water and rheological properties of cellulose nanofiber dispersion, transparent cellulose hydrogel (TCG). Polymer Journal. 2004;**36**:684-694

[35] Felby C, Thygesen LG, Kristensen JB, Jørgensen H, Elder T. Cellulose–water interactions during enzymatic hydrolysis as studied by time domain NMR. Cellulose. 2008;**15**:703-710

[36] Froix MF, Nelson R. The interaction of water with cellulose from nuclear magnetic resonance relaxation times. Macromolecules. 1975;**8**:726-730

[37] Poletto M, Ornaghi HL, Zattera AJ. Native cellulose: Structure, characterization and thermal properties. Materials. 2014;**7**:6105-6119

[38] Morán JI, Alvarez VA, Cyras VP, Vázquez A. Extraction of cellulose and preparation of nanocellulose from sisal fibers. Cellulose. 2008;**15**:149-159

[39] Vermaas JV, Petridis L, Qi X, Schulz R, Lindner B, Smith JC. Mechanism of lignin inhibition of enzymatic biomass deconstruction. Biotechnology for Biofuels. 2015;**8**:1-16

[40] MacKay AL, Wallace JC, Sasaki K, Taylor IE. Investigation of the physical structure of the primary plant cell wall by proton magnetic resonance. Biochemistry. 1988;**27**:1467-1473